**Open Access** 

# Subsurface Characterization in Rugged Himalayan Terrain Using 2D ERT: Implication for Hydropower Development in Karnali, Nepal

Kapil Karki<sup>1\*, 3</sup>, Gyanendra Raj Sapkota<sup>2, 3</sup>, Dilandra Raj Pathak<sup>3</sup>, Rishi Raj Baral<sup>4</sup>, Praveen Upadhyay Kandel<sup>5</sup>, Faraz Ul Haq<sup>6</sup>, and Muhammad Fahim Aslam<sup>6</sup>

<sup>1</sup>Department of Earth Science, The University of Memphis, 3720 Alumni Ave, Memphis, TN 38152 <sup>2</sup>Department of Geosciences, Texas Tech University, 1200 Memorial Circle, Lubbock, TX 79409, USA <sup>3</sup>Quartz Group Pvt. Ltd., Kirtipur, Nepal

> <sup>4</sup>Explorer Geophysical Consultants Pvt. Ltd., Kathmandu 44600, Nepal <sup>5</sup>Geotech Solutions International, Dhobighat, Lalitpur, Nepal <sup>6</sup>Department of Civil Engineering, The University of Memphis, TN, 38152, USA

> > (\*Corresponding E-mail: kkarki@memphis.edu)

Received: January 25, 2025, Accepted: June 25, 2025

Abstract: Hydropower development in the tectonically active and geologically complex Himalayan region requires advanced geophysical methods capable of resolving subsurface heterogeneity in rugged terrain. Twodimensional Electrical Resistivity Tomography (2D ERT) is particularly effective in such environments due to its adaptability, resolution, and ability to delineate lithological and structural variations. In Nepal, ERT has become an essential tool for assessing overburden thickness, bedrock quality, aquifer characteristics, and potential instability zones critical for hydropower development. This study presents the application of 2D ERT at the proposed Peaking Run-of-River (PROR) hydropower project in the Mugu Karnali highlands of western Nepal. Sixteen high-resolution resistivity profiles were collected using the Wenner array with 5 m electrode spacing to image the subsurface. The results reveal distinct resistivity values from very low to very high (20  $\Omega$ ·m - 4,500  $\Omega$ ·m) corresponding to colluvium, weathered bedrock, and competent crystalline formations, including schist, quartzite, and granitic gneiss. Fractured and saturated bedrock zones were also identified, providing insights into site stability and foundation suitability. The resistivity models confirm that the project area possesses competent bedrock conditions appropriate for key hydropower structures. The successful application of ERT in this high relief, folded, and thrusted Himalayan setting underscores its reliability for geotechnical hydropower feasibility studies. These demonstrate that integrating geophysical methods like ERT into project planning enhances the accuracy of subsurface evaluation and supports sustainable hydropower development in rural Nepal.

**Keywords: 2D Electrical resistivity tomography (ERT),** Wenner array, Peaking run-of-river, Hydropower.

#### Introduction

The Himalayan range, stretching over 2,400 km, has been pivotal in advancing our understanding of mountain belt formation, primarily driven by the collision of continental plates (Argand, 1924; Dewey and

Bird 1970; Powell and Conaghan, 1973; Le Fort, 1996; Kohn, 2014). Rugged mountain regions serve as critical components of the global hydrological system and are often described as "natural water towers" due to their capacity to capture, store, and release freshwater (Viviroli and Weingartner, 2008). Tectonic convergence in many of these regions has created high-relief, steep terrains that offer ideal topographic conditions for harnessing water's kinetic energy. Although mountain regions cover only about 32% of global river basin areas, they contribute more than 60% of total discharge, emphasizing their disproportionate role in water supply (Viviroli et al., 2007).

Globally, several countries have effectively utilized the topographic advantages of rugged terrain to generate substantial amounts of renewable energy. China's Three Gorges Dam, the world's largest hydropower facility (22,500 MW) (USGS, 2018; Kumar, 2022; NS Energy, 2025) is situated in a steep gorge along the Yangtze River. In South America, the Itaipu Dam (14,000 MW), jointly operated by Brazil and Paraguay, exploits the Paraná River's gradient and rugged terrain to supply a substantial share of regional electricity. Similarly, Europe's Glendoe Hydroelectric Scheme in the Scottish Highlands utilizes a 600-meter head across steep mountainous terrain to generate 100 MW of electricity (SSE, 2009). In South Asia, India's Bhakra-Nangal Dam, situated in the lower Himalayas along the Sutlej River, utilizes the natural valley topography to generate 1,325 MW (CWC, 2017). Likewise, the Upper Tamakoshi Hydroelectric Project (456 MW), located in the highlands of Dolakha District, capitalizes over 800 meters of hydraulic head from glacial rivers descending steep Himalayan slopes (NEA, 2020).

Nepal presents a textbook example of how mountainous topography facilitates hydropower development. Nepal's rugged terrain is intersected by approximately 6,000 rivers draining a total area of

194,471 km<sup>2</sup>. Of these, 33 rivers have drainage basins exceeding 1,000 km<sup>2</sup>, offering a theoretical hydropower potential of 83,000 MW, of which only about 2% has been developed (Sharma and Awal, 2013; Alam et al. 2017), where 43000 MW is technically and economically achievable (WECS, 2019). Nepal's hydropower potential varies across its provinces due to differences in topography. Nepal is divided into seven provinces, among which Province 1 (Koshi) and Province 6 (Karnali) have the highest potential, with capacities of 22,820 MW and 17,799 MW, respectively. In contrast, Province 2 (Madesh) has the lowest potential, totaling only 341 MW). Nepal's energy capacity surpluses to 3602 MW as of 2025, March (economic survey 2025/2026), with the continued expansion of electricity generation capacity, Nepal is prioritizing the implementation of smart grid technologies to decarbonize the energy sector, enhance grid efficiency, and facilitate the integration of renewable energy sources. As a part of this broader shift toward sustainable and resilient clean energy, new projects are being proposed on high terrain having high gross head for a peaking run of river (PROR), which is supported by geophysical investigations, including 2D electrical resistivity imaging, to assess terrain suitability for infrastructure development and this study will help understand the feasibility of this hydropower project in rocky topography.

Several geophysical techniques could potentially be applied to investigate geological structures near the surface (Epting et al., 2009). Subsurface geological investigations are carried out for a range of purposes including engineering construction, groundwater exploration, seismic activity monitoring (Acworth, 1987; Burger and Burger, 1992; Mukhopadhyay et al., 2006; Satyabala and Bilham 2006; Hassan Imam et al., 2013), geotechnical investigations (Suzuki et al. 2000; Kneisel, 2006; Chambers et al., 2006; Cardarelli et al., 2007; Thompson et al., 2017; Lin et al., 2018), karst features (McGrath et al., 2002; Khalil 2006), landslide slope stability assessment (Jhinkwan et al. 2023; Sigdel et al. 2025) and few investigation focused on case studies of dam inspections (e.g, Wise'n et al. 2000; Karastathi et al., 2002; Al-Fares, 2011). Geophysical data have been widely used in hydrology to find and map underground geological structures such as fault zones (Rehfeldt et al., 1992; Rubin et al., 1992; Hubbard and Rubin, 2000; Lapenna et al., 2005; Singha et al., 2015; Soupois et al., 2007; Colangelo et al. 2008; Gélis et al. 2010; Binley et al., 2015). The adoption of modern geophysical techniques in mountain geomorphology accelerated due to their efficiency, minimally invasive nature, and capacity to deliver high-resolution subsurface information relative to conventional drilling (Demanet et al., 2001). Advances in acquisition and processing now permit precise characterization of nearsurface lithology in structurally complex terrains (Kneisel, 2006), substantially expanding the analytical and applied potential of geophysical investigations (Huayllazo et al., 2023; Nassim et al., 2024). Different geophysical tools have been adopted for studying the

hydropower potential in Nepal Himalaya, among them 2D ERT is highly applied techniques in identifying the feasible location for the hydropower components. Pant (2005), Ghimire et al. (2017), Lamsal et al. (2020) Takamte et al. (2022) used the 2D ERT method to delineate subsurface geological structures for hydropower studies. Silwal and Paudyal (2018) also used this method to identify the subsurface lithology of Dotigad hydropower project with different hydraulic components. Adhikari et al. (2019), Mebrahtu (2019), Srivastava et al. (2022), and Acharya et al. (2023) also used this technique for investigating the subsurface geology for hydropower dam site suitability and rehabilitation.

Despite considerable advancements in hydropower exploration across Nepal, the remote Karnali province remains largely under-investigated, and its subsurface characteristics pertinent to energy development are poorly constrained. While hydropower feasibility studies have proliferated in more accessible regions, detailed geophysical assessments in Karnali are sparse, and no systematic Electrical Resistivity Tomography (ERT) investigations have been conducted along key river segments. In this study, ERT has been applied to selected sites along the Mugu Karnali River to characterize subsurface lithologies, identify fractured or weathered bedrock, and assess geotechnical stability. The resulting high-resolution subsurface models not only inform local hydropower feasibility but also provide insights into broader geological and hydrogeological conditions of the region, offering a framework for future energy development and geotechnical investigations in similar underexplored segments of Karnali.

# **Study Area**

#### **Geology of the Area**

Karnali valley (Figure 1) extends The Mugu approximately E-W and offers about 30-40 km of almost uninterrupted exposure of the primary tectonometamorphic units (Montomoli et al. 2013). The project area is located within the Higher Himalayan Sequence (HHS) and is near the Main Central Thrust (MCT) zone. The Galwa Tectonic Window is surrounded by a geological formation dominated by two-mica gneiss, quarzitic gneiss, quartzite, garnet-kyanite-mica schist or gneisse, amphibolite, and calc-gneiss of the Higher Himalaya. Above this sequence lies a thick layer, extending several thousand meters, consisting of granite-gneiss, migmatite, paragneiss, and carbonate rocks. Kyanite, typically found in the lower parts of this sequence, transitions to sillimanite in the higher elevations (Fuchs, 1974). In the northern part of the Higher Himalayan crystalline region, there is an intrusion by Mugu Granite (Hagen, 1969).

The Mugu Granite exhibits a medium-grained texture characterized by hypidiomorphic crystals. Notably, it contains twinned and zoned microcline phenocrysts,

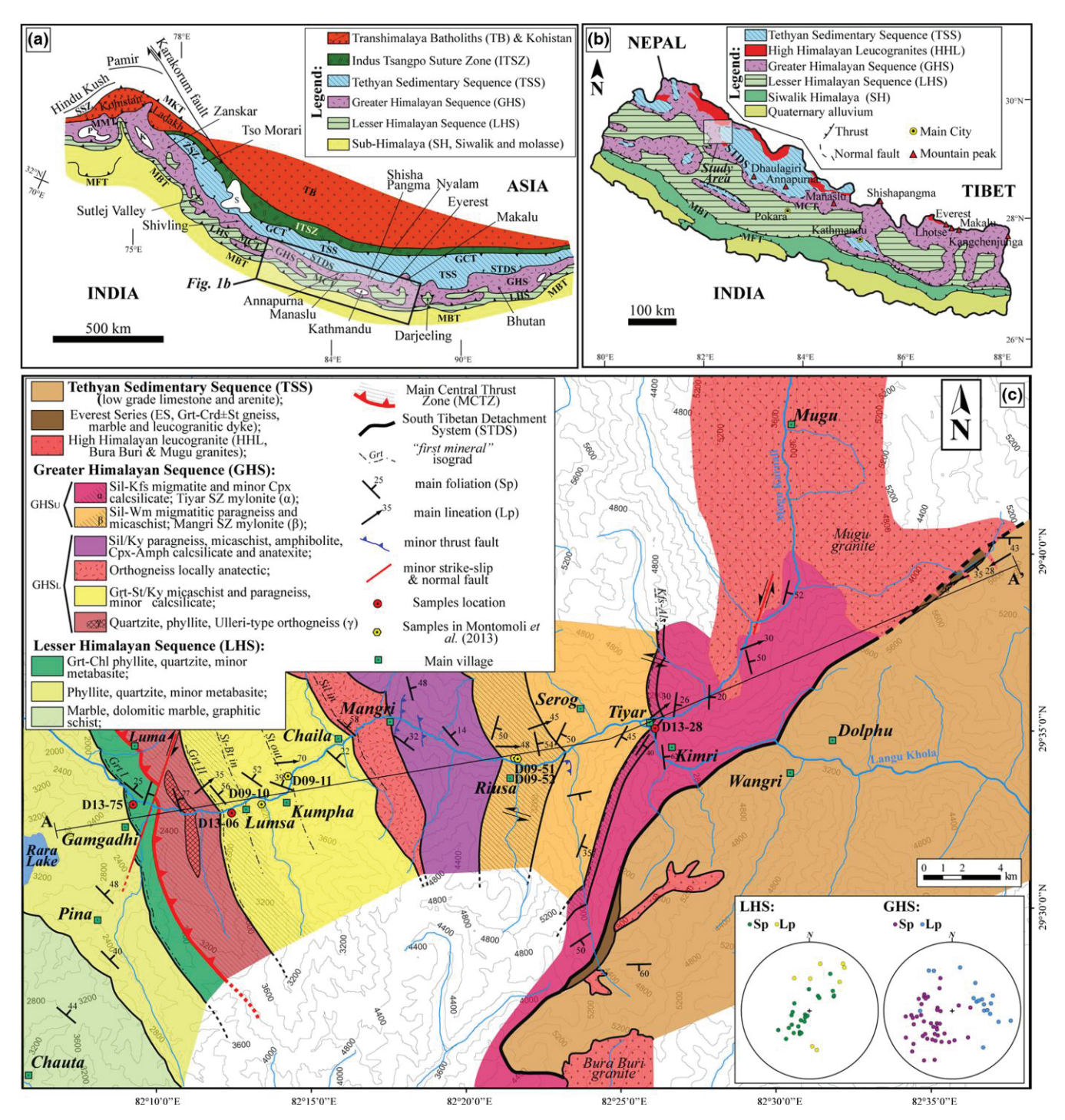


Figure 1, (a) Geological map of the Himalayan range (after Law et al. 2004). The approximate location of (b) is reported; (b) geological map of the Nepalese Himalaya (after Montomoli et al. 2013 and references therein). The Mugu Karnali valley (study area) is shown; (c) Tectono-metamorphic map of the Mugu Karnali valley (Western Nepal). For simplicity, only samples cited in the text or in Montomoli et al. (2013) are indicated. Cross-section trace (A–A') of Fig. 2 is shown. In the inset, stereo plots of the main structural elements of LHS and GHS are reported (Wulff net – lower hemisphere). SSZ, Shyok suture zone; ZSZ, Zanskar shear zone; MKT, Main Karakoram Thrust; MMT, Main Mantle Thrust; TB, Tibetan Block; ITSZ, Indus Tsangpo Suture Zone; GCT, Great Counter Thrust; TSS, Tethyan Sedimentary Sequence; GHS, Greater Himalayan Sequence; STDS, South Tibetan Detachment System; MCT, Main Central Thrust; MBT, Main Boundary Thrust; MFT, Main Frontal Thrust; K, Kashmir basin; P, Peshawar basin; S, Sutlej basin.

some reaching lengths of up to 1 cm, which encapsulate plagioclase, biotite, muscovite, and sporadic occurrences of sillimanite oriented parallel to the zoned peripheries of potassium feldspar (K-feldspar) (Fuchs, 1977). The boundary between the Mugu Granite and the migmatite complex is gradual rather than distinct. Migmatization processes were partially influenced by the intrusion of the Mugu Granite, evidenced by migmatites hosting older augen gneisses and some paragneisses intersected by folded veins of granite. Conversely, the granite itself contains numerous xenoliths of augen gneiss (Fuchs, 1977).

The Higher Himalayan Sequence (GHS) is positioned above the Lesser Himalayan Sequence (LHS) and serves as the metamorphic core of the Himalayan mountainbuilding process. The LHS is bordered to the south by the Main Boundary Thrust (MBT) and to the north by the Main Central Thrust (MCT), both of which trend approximately northwest-southeast and dip towards the northeast, roughly perpendicular to the mountain range's orientation (Colchen and Le Fort, 1986; Le Fort, 1975). The uppermost layer of the granite is composed of a sequence including calc-gneiss, marble, calcschist, and calc-phyllite. These rocks belong to the lower section of the Dhaulagiri Limestone, with a decrease in metamorphic grade observed as one move upwards in the stratigraphy. The Higher Himalayan crystalline in this region exceeds a thickness of 10 km (Fuchs, 1974).

The proposed site lies in Mugu District of Karnali Province (Figure 2). The project layout consists of a 27 m high gated barrage, 16497.26 m, and a 7 m diameter in horseshoe shaped tunnel on the right bank of the river, a 20 m Dia and 66.49 m high surge shaft (circular orifice concrete-restricted type) and powerhouse: housing four generating units of 70.59 each. The proposed run-of-river project is a high head project with an installed capacity of 306 MW, which is in Mugum Karmarong Rural Municipality and Chhayanath Rara Municipality shown in Figure 2. The headworks area is located at Mugum Karmarong Rural Municipality ward number 3 and powerhouse area is located at Chhayanath Rara Municipality ward number 12. The proposed project lies between 82° 13' 45" E to 29° 32' 46" N and 82° 25' 55" E to 29° 35' 50" N.

#### **Stratigraphy**

Stratigraphically, the project area is divided into the following units (Figure 3).

#### **Lumsa Unit**

This unit is exposed around Lumsa Village and falls into Lesser Himalayan Sequence separated from Higher Himalayan Crystalline by the MCT. The lithology of the unit consists of thinly foliated, fine-to medium-grained,

slightly to moderately weathered grey schist with intercalated thin-bedded, medium-grained, moderately weathered light grey micaceous quartzite containing quartz veins. The mineral assemblage includes quartz, feldspar, mica, and garnet. The thickness of this unit exceeds 3 km.

#### **Chhaila Unit**

This unit falls under Higher Himalayan Crystallines above the MCT. The rock types include schist and quartzite with occasional concordant intrusion of amphibolite. The schist contains abundant garnets of size up to 1 cm. Kyanite flakes are also developed on quartz veins. Malachite mineralization is also present on quartzite at some localities. The thickness of this unit is 4.5 km.

#### **Mangri Unit**

This unit is widely distributed around Mangri Village. The lithology consists of thin-to medium-foliated, thin-to thick-banded, coarse-grained, slightly weathered, medium strong to strong light grey granitic gneiss with partings of weak grey mica schist. The mineral assemblage consists of quartz, feldspar, mica, and tourmaline in granitic gneiss. Schist contains quartz, feldspar, and mica. The thickness of this unit is 5.5 km.

#### **Darima Unit**

This unit is well exposed around Darima Village at roadcut sections, river-cut sections and hills and ridges. The rock types include medium-to massive-bedded, coarse-grained, jointed, moderately to slightly weathered, grey and pink quartzite with coarse-grained, moderately weathered weak grey schist partings. Steep cliffs are developed due to the presence of strong quartzites at this unit. The thickness of this unit is 1.5 km.

#### **Pulu Unit**

This unit is well exposed around Pulu Village. The lithology consists of thin- to medium-foliated, coarse-grained, thick to massive-banded, slightly to faintly weathered grey banded gneiss with migmatite, granitic gneiss and occasional thin-bedded grey quartzites. The strata are generally north dipping. Quartz boudins and M-type folds are abundant on quartz veins which are both parallel and oblique to foliation planes. The thickness of this unit is more than 1.2 km.

# Methodology

#### **ERT** survey

Electrical resistivity methods have wide advantage of efficiency and adaptability to topography and become a mature tool for subsurface study (Wu et al. 2023).

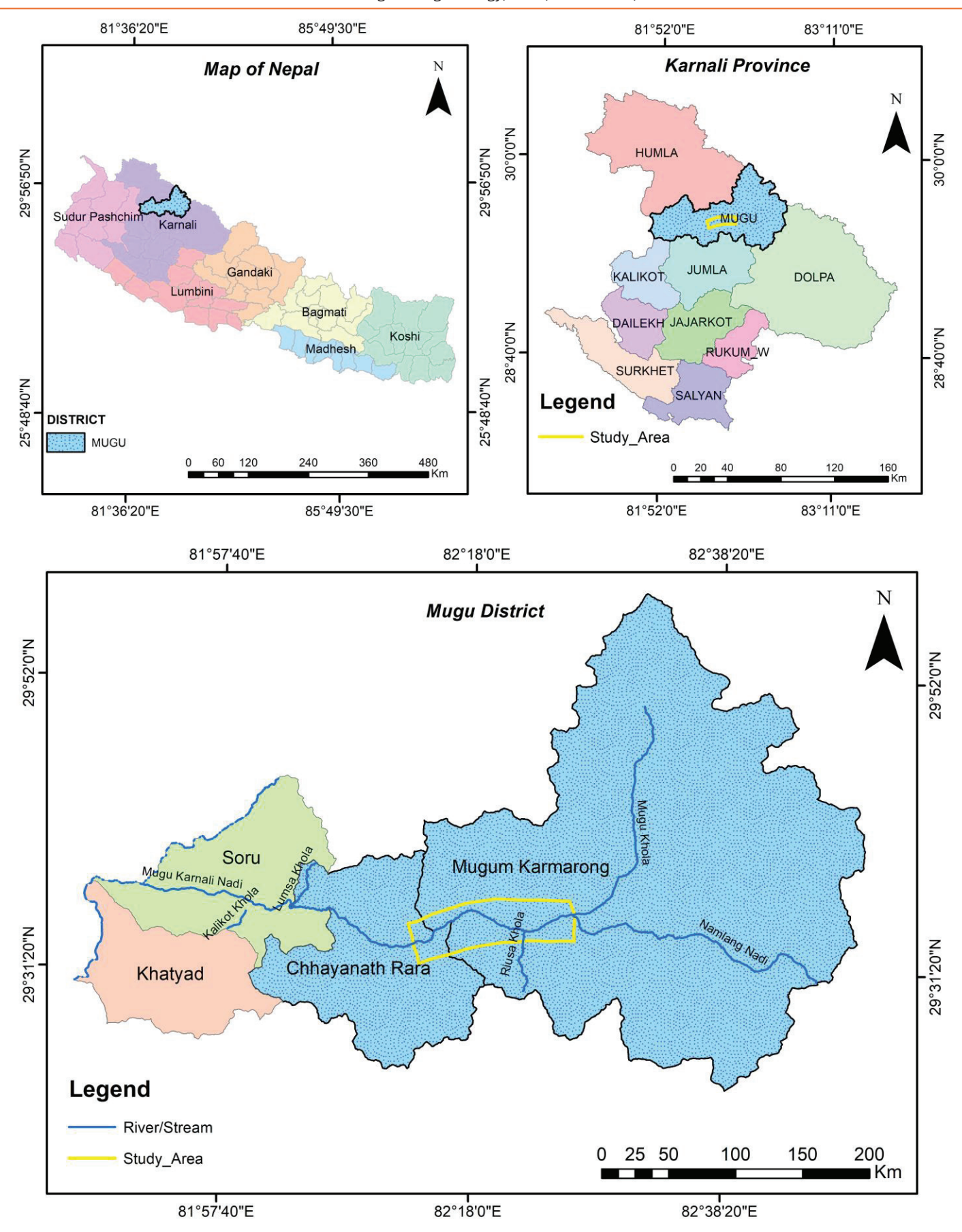
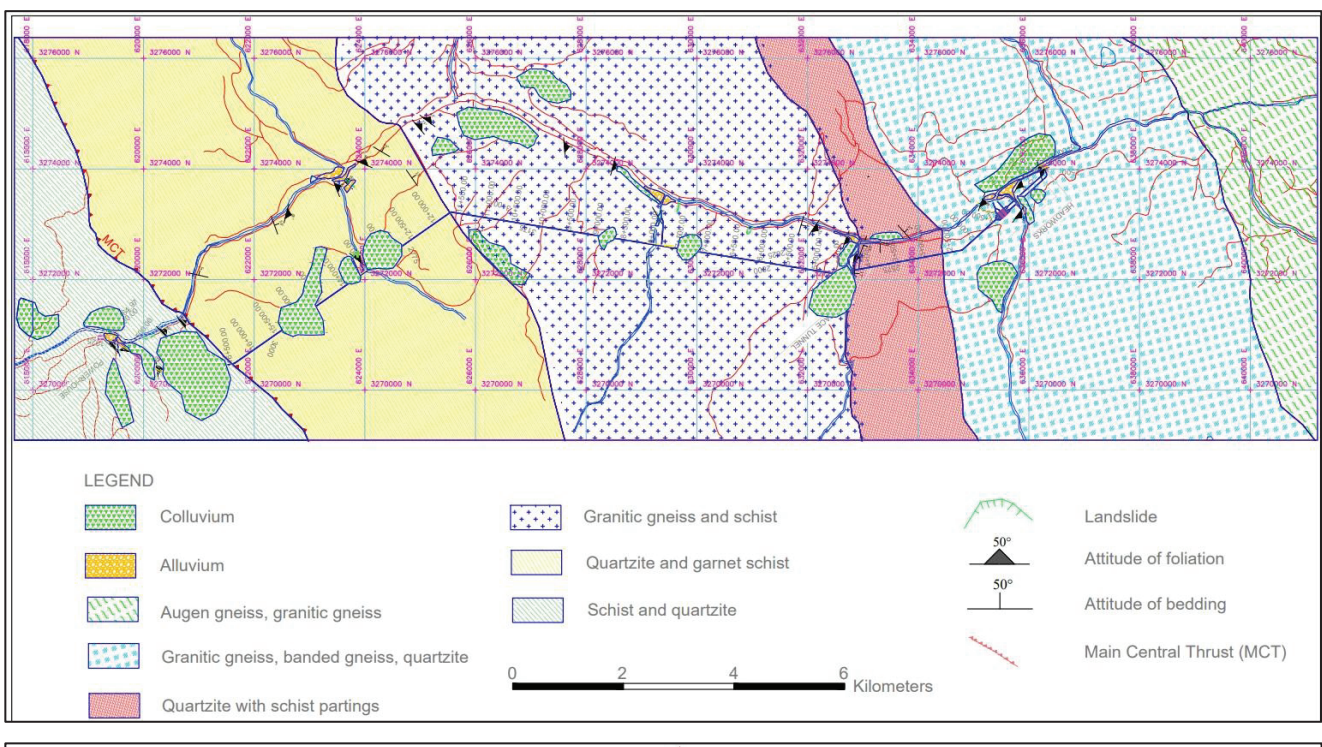


Figure 2, Location map of study area.



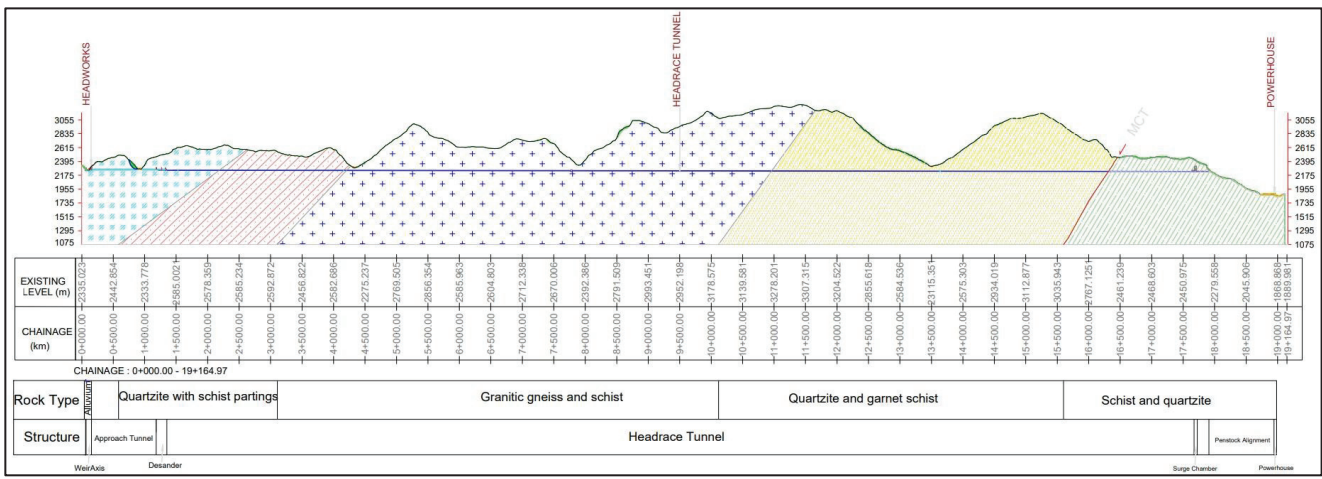


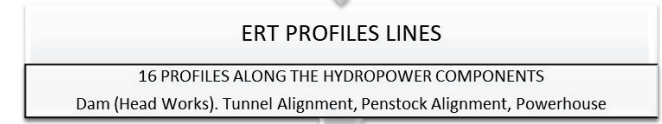
Figure 3, Engineering geological maps and geological cross-section along the project area.

Geophysical methods have a wide range of applications in locating or tracing an object of interest as suggested by the geophysical response to the object. In ERI surveys, electrical resistivity is recorded (measured in  $\Omega$ representing the reciprocal of electrical conductivity. Resistivity Imaging is a geo-electrical method utilized for acquiring detailed 2D and 3D images of intricate subsurface geology (Griffiths and Barker, 1993). This technique involves deploying various electrode configurations such as Wenner, Schlumberger, dipole-dipole, pole-dipole, pole - pole (Dobrin, 1982). In surface ERT applications, electrodes are often installed in a straight-line arrangement using multicore cables. The Wenner array method was selected because of its strong resistance to noise and reliability in outlining horizontal subsurface features (Falae et al., 2019). According to Dobrin (1982), the method detects changes in subsurface geology by evaluating the apparent resistivity, which indicates variations in electrical resistivity. Samouëlian et al. (2005) offer an in-depth explanation of the theory and fundamental principles underlying ERT.

The fundamental principle of ERT relies on the varying electrical conductivity of subsurface materials, which is influenced by numerous factors. These factors include rock type, porosity, permeability, pore connectivity, temperature, salinity, cation exchange capacity, clay content, the nature of fluids or water present, degree of weathering, presence of fractures or faults, discontinuities (Hao et al., 2002; Tejero et al., 2002; Kim et al., 2007; García-Moreno and Mateos 2011; Cardarelli et al., 2010; Ha et al., 2010; Lech et al., 2020), rock associations, deformation, and water-rock interactions or alterations. (Aizebeokhai et al., 2010, Hasan et al., 2018, Hung et al., 2020). In hard rock terrains, electrical resistivity can vary over a large range

depending on weathering degree, water saturation, etc. (Hasan et al., 2020). ERT generates an image of subsurface resistivity, which can be interpreted to infer different lithologies or rock types based on their resistivity contrasts (Hasan et al. 2020). The outline of the methodology for subsurface characterization is given in the flow chart (Figure 4).





|                      | resitivity imaging                  |  |
|----------------------|-------------------------------------|--|
| RESITIVITY INVERSION | CLASSIFICATION &<br>LAYERING STRATA | DEPTH, MATERIAL<br>CHARACTERISATION AND<br>LITHOLOGICAL UNITS) |

Figure 4, Methodology flow chart for subsurface characterization.

# **Data acquisition and processing**

Data acquisition was carried out by using equipment known under the brand name GEOMATIVE GD10 SUPREME 2D PLUS MULTI-ELECTRODE RES/IP IMAGING SYSTEM manufactured by GEOMATIVE CO., LTD., China. The ERT imaging setup is depicted in Figure 5. During the investigation, 60 electrodes were linked by two cables, spaced at 5 m distances arranged in straight lines (Cubbage et al., 2017) giving maximum of 300 m length following the guideline set by Loke and Barker (1996). A total of sixteen ERT profiles were used for site characterization, denoted as ERT-1 to ERT-16. To reduce electrode spacing errors, two technicians verified electrode placement before each survey, and salt water was applied to improve ground contact. A reconnaissance survey ensured equipment and configuration reliability. In noisy areas, measurements were repeated 2-3 times for accuracy. Topographic elevations and geographic coordinates were recorded by total station at each electrode for spatial referencing and model correction (Table 1).

The instrument is fully automatic and designed to measure apparent resistivity as well as induced polarization of the subsurface materials. In a noisy area, the signal is significantly enhanced by stacking data measured in many cycles (4-10 stacks). It consists of three main units all housed in a single casing: the transmitter, the receiver, and the microprocessor. The electrically isolated transmitter sends out well-defined and regulated signal currents.

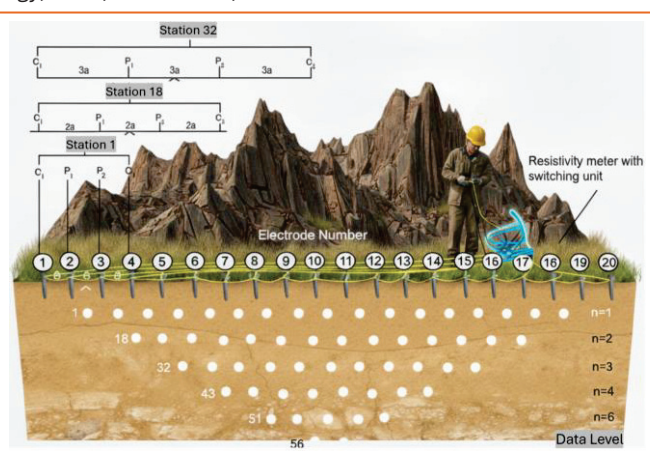


Figure 5, Schematic diagram of a multi-electrode system, and a possible sequence of measurements to create a 2-D pseudo section. (modified after Loke et al., 2013).

The receiver discriminates against noise and measures voltages correlated with transmitted signal current. The microprocessor monitors and controls operations and calculates results. The apparent resistivity is calculated automatically and displayed in digital form. Stainless steel electrodes (30 cm long) were used for both current transmission and voltage receiving. These electrodes were grounded in each profile and related to the Geomative GD-10 by specially designed CA30 ERT cables.

The inversion routine employed by the RES2DINV program relies on the smoothness-constrained least squares method (De Groot-Hedlin and Constable, 1990; Saski, 1992). Pre-processing of data to obtain a highquality data set is followed by tomographic inversion. Data inversion code is another main component of the 2D-ERT method. A popular inversion algorithm, RES2Dinv, created by Loke and Barker (1996) and improved by Loke et al., 2003, works using a leastsquares method with smoothness constraints. Geological interpretation of the resistivity tomogram is based on geometry along with resistivity values of such patches. Surface layers and/or geological, hydrogeological, geomorphological information play key roles during the interpretation of the resistivity tomograms and are interpreted with reference to established resistivity (Figure 6).

To improve the clarity and resolution of the resulting models, RMS error statistical analysis was utilized to filter out noise and data artifacts prior to processing (Miller et al., 2008). Post-inversion datasets with high RMS error values were discarded, most likely due to poor electrode-ground contact. Rucker et al. (2011) define absolute error as the absolute deviation between two repeated measurements. Each inversion included at least seven iterations, and only those with RMS errors below 10.0 were retained for interpretation.

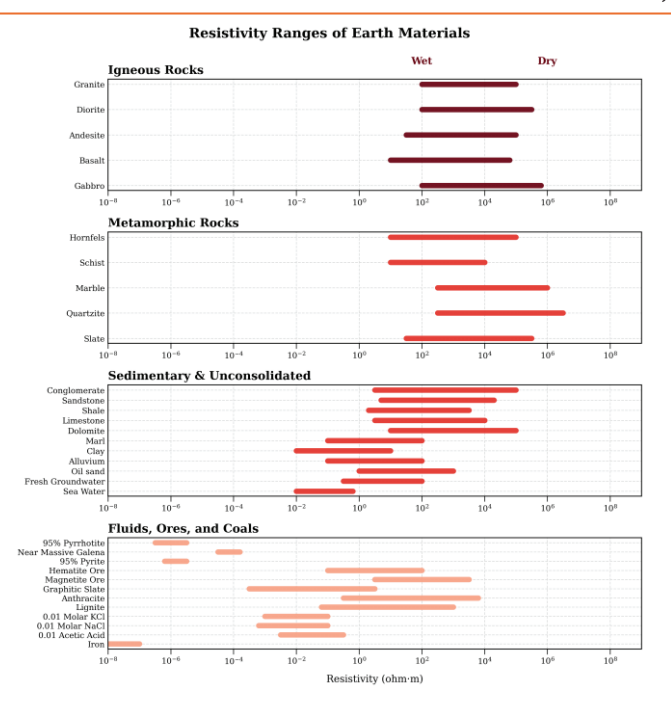


Figure 6, Electrical conductivity and resistivity of various rocks, soils and minerals (modified after Telford et al., 1990).

Table 1, ERT surveys with RMS error lower than 10%.

| Profile | Length<br>(m) | Data<br>Points | RMS<br>Error      | Profile | Length<br>(m) | Data<br>Points | RMS<br>Error |
|---------|---------------|----------------|-------------------|---------|---------------|----------------|--------------|
| ERT-1   | 300           | 371            | <b>(%)</b><br>8.3 | ERT-9   | 300           | 533            | 4.4          |
| ERT-2   | 300           | 548            | 2.5               | ERT10   | 300           | 554            | 4.3          |
| ERT-3   | 300           | 510            | 6.1               | ERT11   | 300           | 410            | 8            |
| ERT-4   | 300           | 527            | 6.2               | ERT12   | 300           | 518            | 8.1          |
| ERT-5   | 300           | 521            | 4                 | ERT13   | 300           | 379            | 7.7          |
| ERT-6   | 300           | 527            | 4                 | ERT14   | 150           | 119            | 7.2          |
| ERT-7   | 300           | 545            | 2.4               | ERT15   | 150           | 99             | 9            |
| ERT-8   | 150           | 117            | 6.2               | ERT16   | 150           | 135            | 6.2          |
|         |               |                |                   |         |               |                |              |

# **Results and Discussion**

#### **ERT Profiles**

The 2D data was inverted into resistivity models, showing both lateral and vertical subsurface resistivity distribution. The models revealed a wide variation of subsurface information. A total of 16 profiles, covering a combined length of 4,100 meters, were surveyed during the investigation. The electrical resistivity survey was carried out along different profile lines in various hydropower components including the reservoir area, adit tunnels, headworks area, intake site, powerhouse, penstock, and tunnel axis (Figure 7). The models reveal a spectrum of resistivity zones, ranging from low to relatively high. Geological materials are categorized based on their resistivity values, with fresh bedrocks, fresh to moderately weathered bedrocks, and weathered bedrocks with minimal fractures.

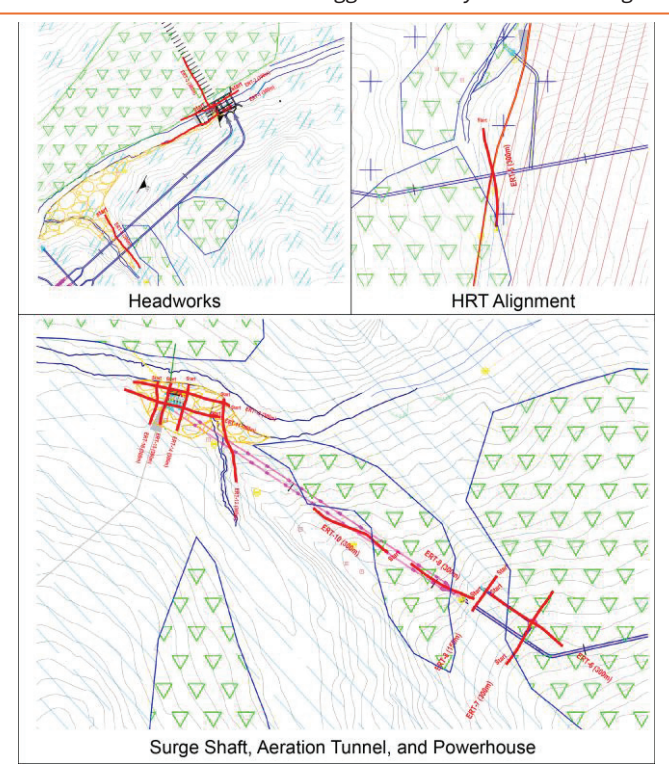


Figure 7, Drawings showing ERT alignments in the surveyed area.

The four ERT profiles conducted in the headworks area reveal consistent subsurface patterns with notable local variations. All profiles show a clear distinction between an overburden layer and underlying fractured bedrock, with varying degrees of saturation and resistivity (Figure 8). ERT-1, conducted along the left bank of the Mugu Karnali River, displays four layers, including thin colluvium and alluvium overlying saturated fractured bedrock with resistivity variations likely reflecting differences in lithology and groundwater presence; field observations support this, with alternating granitic gneiss, banded gneiss, and quartzite. In contrast, ERT-2 and ERT-3, both on the right bank, depict simpler two-layered structures with a moderately thick overburden (3-10 m in ERT-2 and 7-46 m in ERT-3) and low-resistivity, saturated fractured bedrock below, suggesting more uniform subsurface conditions in these locations. ERT-4, carried out along the right bank of Puwa Khola, shows greater lateral variation in the overburden; saturated alluvium dominates the left side (2-8 m thick), while colluvium with mixed resistivity occupies the right (2–12 m thick). Like the others, ERT-4 reveals a fractured, saturated bedrock beneath the overburden. Overall, the profiles consistently identify fractured bedrock as the foundational layer, while variability in overburden thickness, resistivity, and saturation reflect changes in topography, lithology, and proximity to the river.

The ERT profiles ERT-5 through ERT-8, conducted along the right bank of the Riusa Khola and surrounding tunnel zones, consistently delineate a three-layered subsurface structure, albeit with noticeable lateral variations in resistivity and lithology (Figure 9).

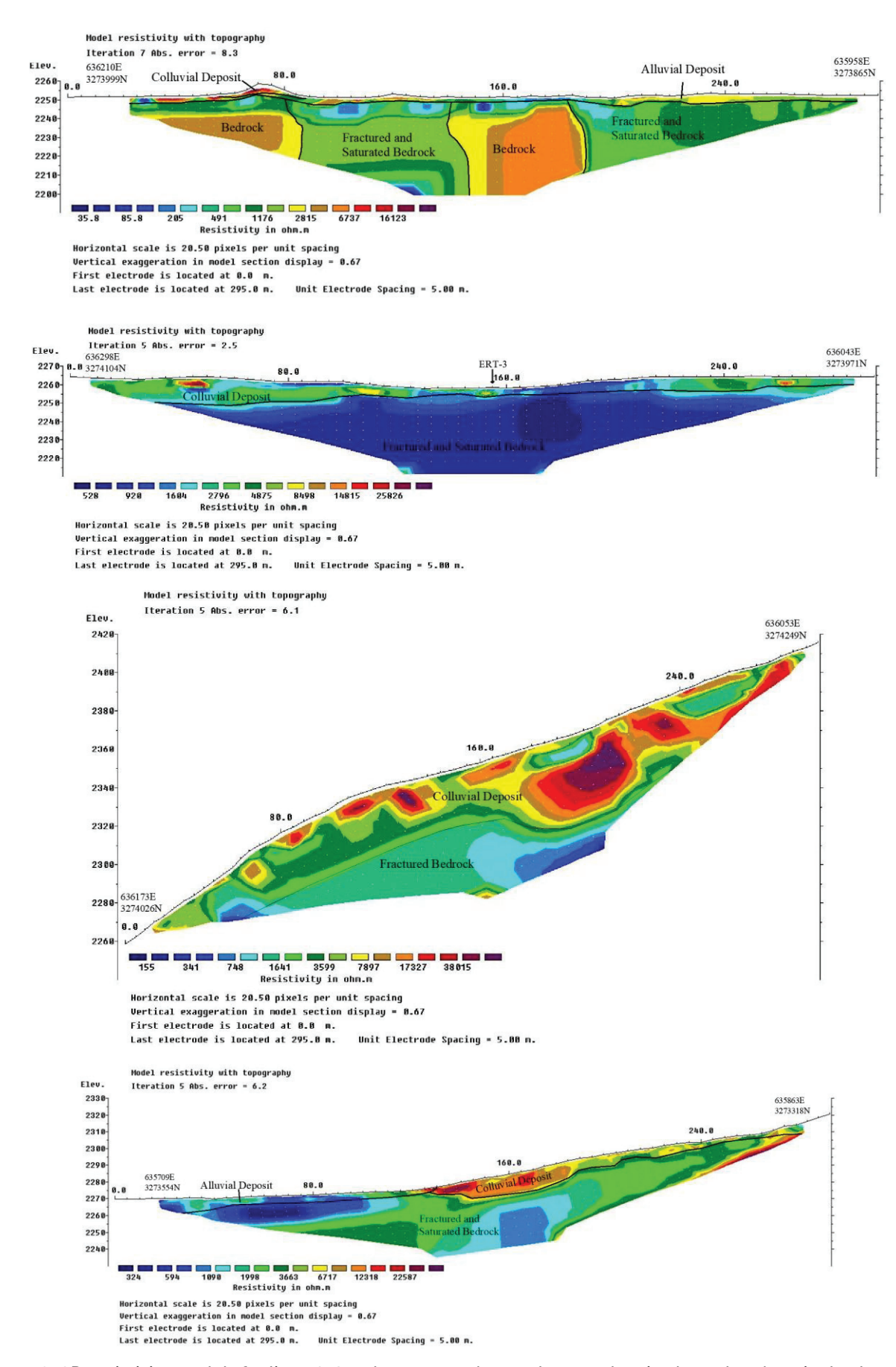


Figure 8, 2D resistivity models for lines 1-4 at the proposed powerhouse, showing lateral and vertical subsurface resistivity variations (5 m inter-profile spacing).

ERT-5, aligned with the headrace tunnel, reveals a 4–11 m thick, dry colluvial overburden, characterized by relatively high resistivity. This layer is underlain by massive granitic gneiss with schist partings, displaying high resistivity values indicative of intact rock conditions. Toward the end of the profile (chainage 182–278 m), the resistivity markedly decreases, suggesting a transition to fractured and weathered bedrock, potentially influenced by seepage or structural weaknesses.

ERT-6 and ERT-7, obtained along the surge shaft hillslope, exhibit a broadly similar subsurface configuration. Both profiles show a thin -to moderately thick colluvial cover of approximately 2-8 m in ERT-6 and 2.5-6 m in ERT-7, overlying moderately weathered bedrock of 11–17 m and 6–16 m thick, respectively. The lowermost layers in both profiles correspond to alternating schist and quartzite horizons, inferred from contrasting resistivity patterns. The deeper section of ERT-6 (chainage 68–255 m) shows relatively low resistivity, reflecting a predominance of schistose material, whereas ERT-7 exhibits higher resistivity, suggesting a greater quartzite content.

ERT-8, located along the aeration tunnel portal, though shorter in length (150 m), also reveals a clear three-layer structure. The uppermost overburden is very thin (~1 m), followed by a moderately weathered bedrock layer (5–11 m thick), and a deeper low-resistivity zone interpreted as interbedded schist and quartzite.

Overall, the ERT-5 to ERT-8 profiles depict a consistent stratigraphic framework—an upper colluvial cover underlain by weathered rock and then more competent bedrock. However, the resistivity variations across the profiles reflect local lithological heterogeneity with quartzite-dominated zones exhibiting higher resistivity, while schist-rich sections are associated with lower values, implying differences in permeability and degree of fracturing.

ERT-9, ERT-11, and ERT-12, each 300 m long and conducted along the penstock alignment near Lumsa Village on the left bank of the Mugu Karnali River, reveal layered but variable subsurface configurations with differing degrees of complexity (Figure 10).

ERT-9 displays a typical three-layer sequence comprising of (i) a heterogeneous colluvial layer (2–7 m thick) with variable but generally high resistivity; (ii) a moderately weathered bedrock zone (5–27 m thick); and (iii) a deeper unit characterized by alternating quartzite and garnet schist, inferred from contrasting resistivity values.

ERT-11 shows a two-layer section, consisting of a thick, variable overburden (2–25 m) composed of loose, unconsolidated materials with sporadic boulders,

underlain by a fractured and saturated bedrock composed of schist and quartzite. A sharp drop in resistivity from chainage 83 m onward marks highly fractured zones, possibly linked to faulting or increased water content.

ERT-12, the most geoelectrically complex of the three, delineates four distinct layers: (i) an upper heterogeneous alluvial layer (up to 27 m thick); (ii) a thin colluvium (<4 m); (iii) a moderately weathered bedrock (3–14 m thick); and (iv) a deep, saturated bedrock layer with low resistivity (<4300  $\Omega \cdot m$ ), interpreted as interbedded schist and quartzite.

Collectively, these profiles confirm the presence of colluvial and weathered/fractured bedrock sequences along the penstock alignment. However, ERT-12 is unique in capturing a deeply saturated bedrock zone beneath thick alluvium, in contrast to the relatively simpler two-layer configuration of ERT-11 and the resistive, quartzite-rich bedrock in ERT-9.

ERT-13 through ERT-16, carried out across the turbine foundation zones near the powerhouse area on the left bank of the Mugu Karnali River, predominantly indicate a two-layered subsurface system (Figure 11). This structure comprises an upper alluvial overburden and an underlying fractured, saturated bedrock.

ERT-13 (300 m) and ERT-14 (150 m), both aligned along the upstream turbine foundations, reveal thick alluvial overburden dominated by boulder- and gravel-rich sediments, ranging from 8–30 m and 4–12 m, respectively. Beneath this layer lies a fractured schist-quartzite bedrock, interpreted from moderate to low resistivity values. ERT-14 demonstrates a relatively uniform overburden distribution with localized resistive anomalies, likely indicating embedded boulders or compact gravel zones.

Similarly, ERT-15 and ERT-16 (each 150 m long) exhibit comparable subsurface conditions, characterized by an upper alluvium layer with heterogeneous resistivity reflecting variable grain size and moisture content. The underlying moderately to highly fractured bedrock shows variable resistivity patterns consistent with alternating schist and quartzite layers.

Across all four profiles, the overburden thickness varies from 2 to 16 m, while bedrock occurs at shallow to moderate depths (approximately 4–26 m). Despite localized resistivity contrasts, the overall interpretation indicates a consistent geological framework within the powerhouse site, comprising of a coarse-grained, thick alluvial cover resting upon fractured and partially saturated bedrock, with spatial variations controlled primarily by lithology and degree of fracturing.

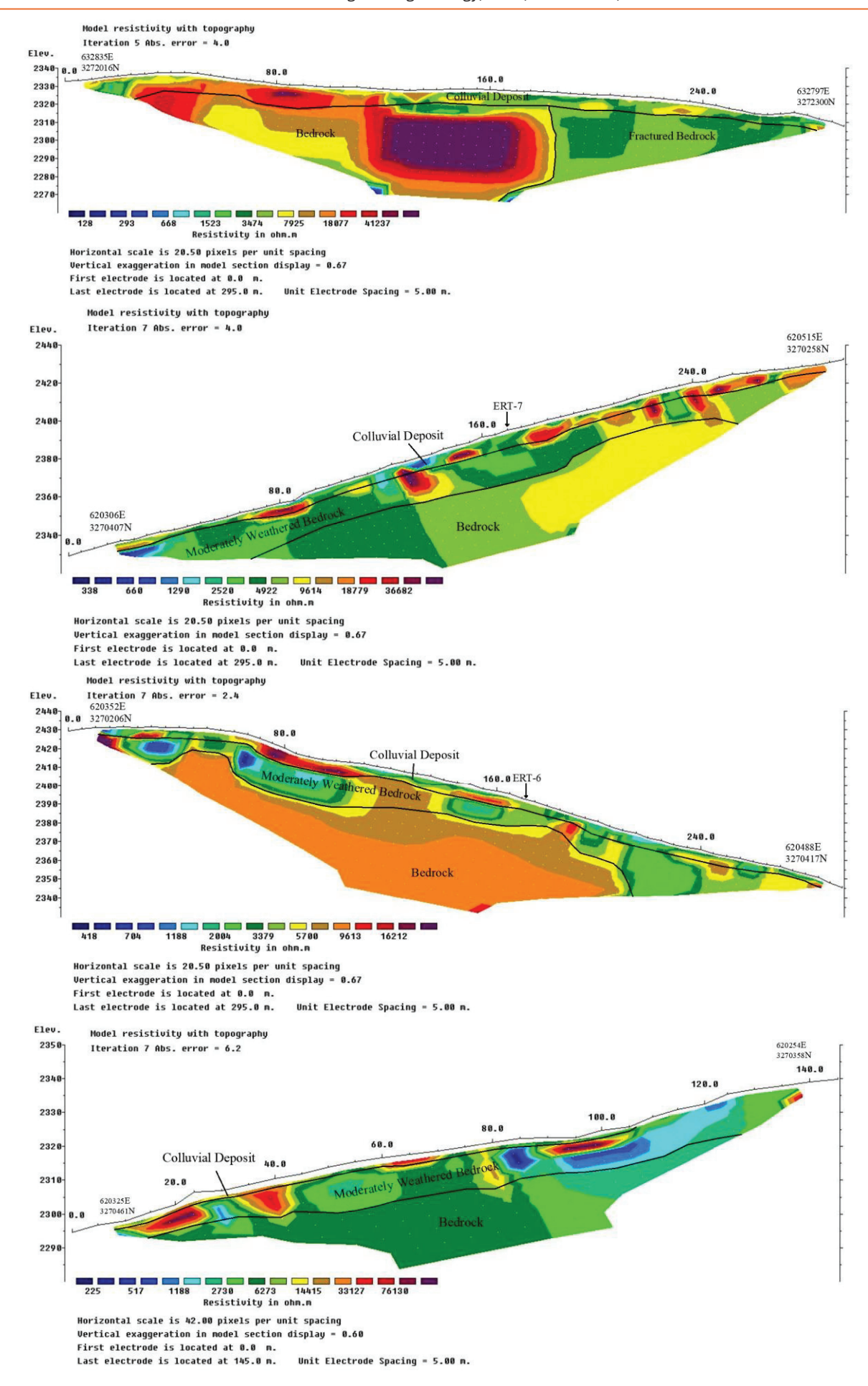


Figure 9, 2D resistivity models for lines 5 - 8 at the proposed powerhouse, showing lateral and vertical subsurface resistivity variations (5 m inter-profile spacing).

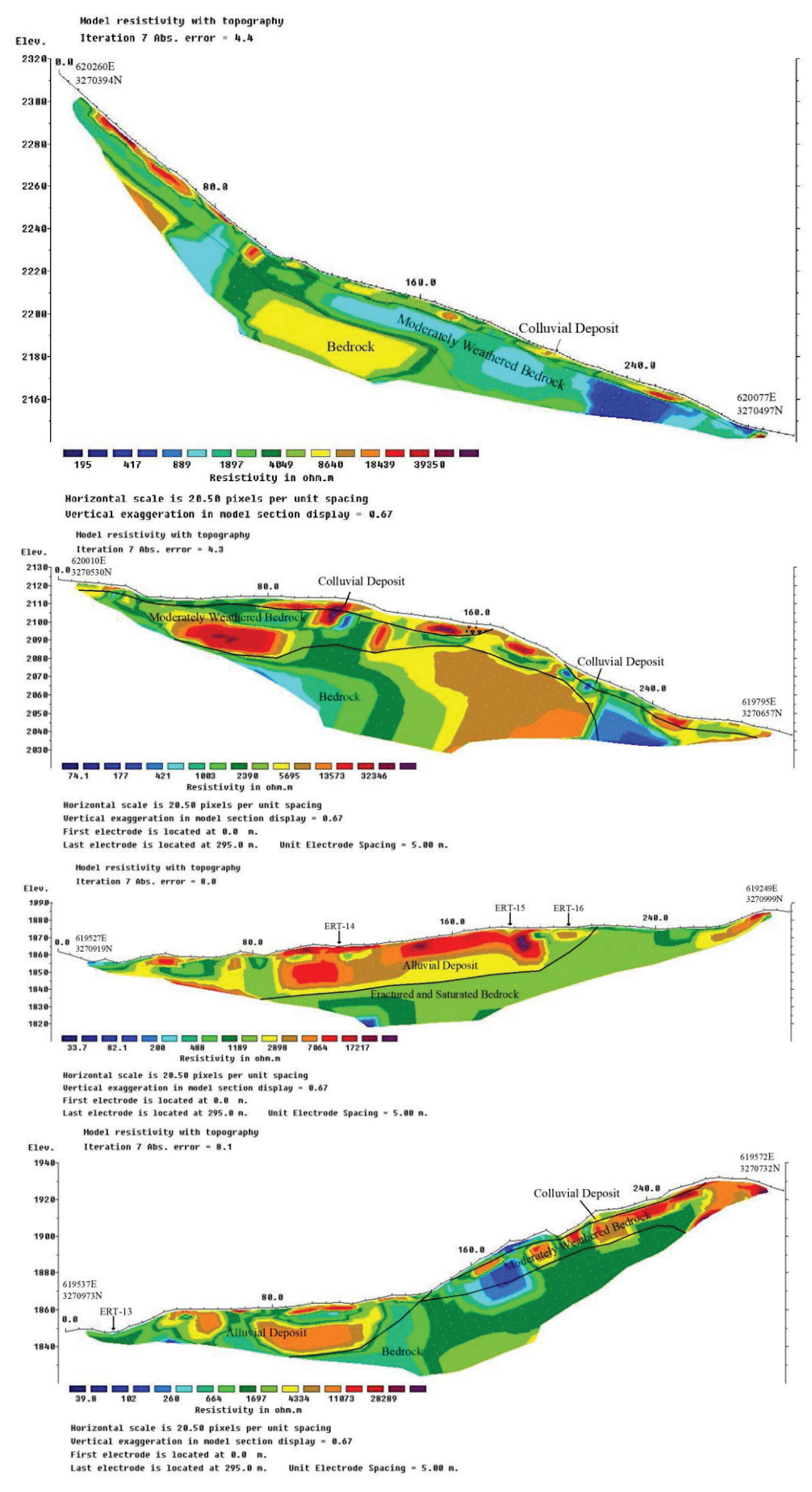


Figure 10, 2D resistivity models for lines 9–12 at the proposed powerhouse, showing lateral and vertical subsurface resistivity variations (5 m inter-profile spacing).

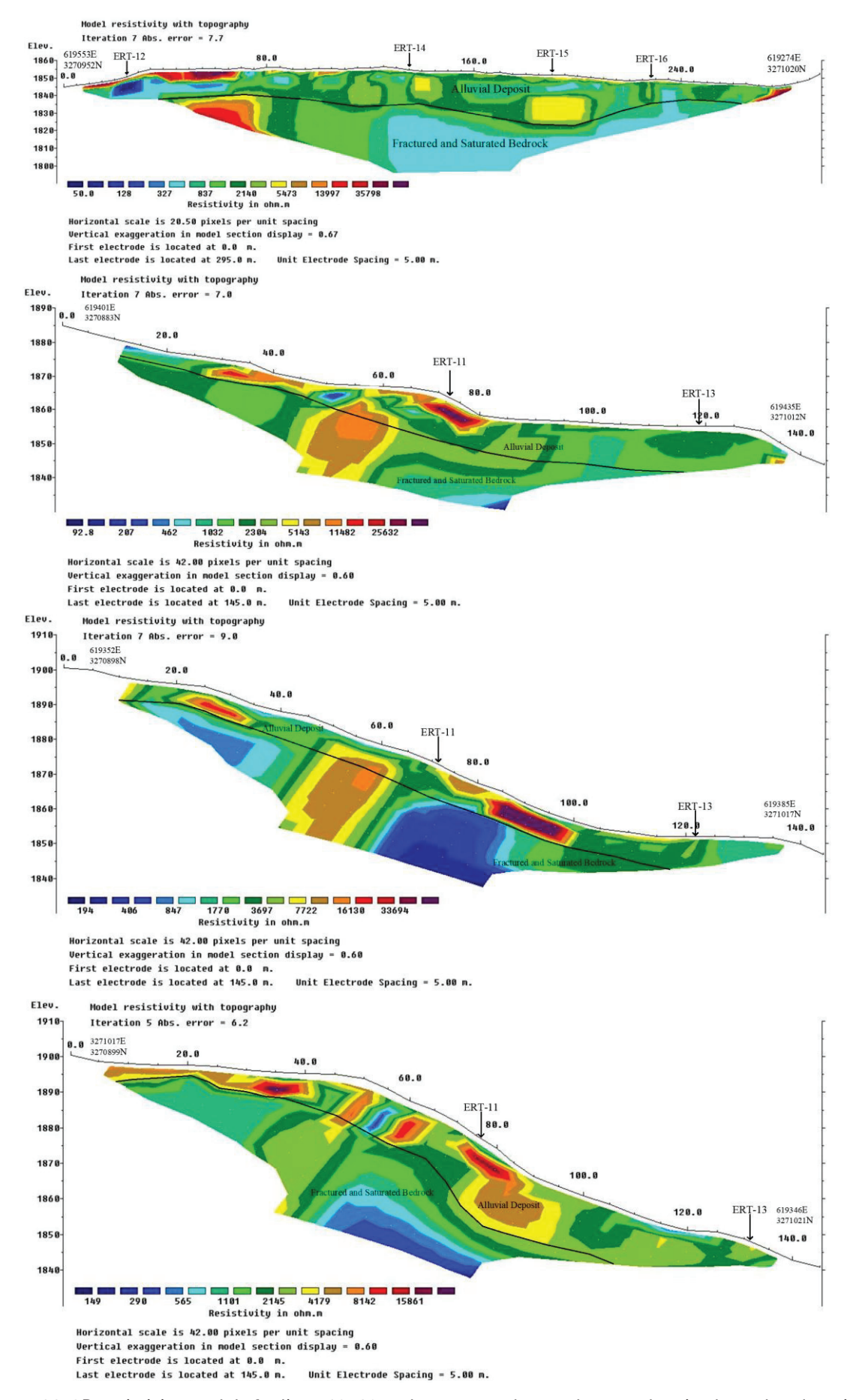


Figure 11, 2D resistivity models for lines 13–16 at the proposed powerhouse, showing lateral and vertical subsurface resistivity variations (5 m inter-profile spacing).

#### **Conclusions**

The results of ERT survey demonstrate its effectiveness as a reliable geophysical method for resolving upper crustal heterogeneities and delineating subsurface geological features in rugged terrain. The field instrumentation, designed to support synchronous voltage measurements across extensive multi-electrode arrays, enabled resistivity profiling over distances exceeding 4 km. The rocks around the project area have three local lithological units such as the schist, quartzite and gneiss.

Based on the resistivity values, the uppermost layer is characterized by relatively low to moderate resistivity  $(20-400 \,\Omega \cdot m)$ , corresponding to unconsolidated colluvial and alluvial sediments with thicknesses ranging from 1 to 46 m. Beneath this, an intermediate resistivity zone  $(1,000-4,500 \Omega \cdot m)$ represents moderately weathered to fresh bedrock, typically 3 to 27 m thick, composed predominantly of schist, quartzite, and granitic gneiss. The basal layer exhibits variable resistivity signatures (<1,000 Ω·m) associated with fractured and saturated competent bedrock, occurring at depths between 4 and 30 m, and reflecting local lithological heterogeneity and groundwater presence.

Moreover, the surveyed area is generally suitable for the proposed hydropower components; however, additional ground-truth investigations such as borehole drilling, in-situ testing, and detailed geotechnical mapping would further validate the ERT interpretations and provide greater assurance for long-term structural stability.

# **Acknowledgments**

The authors thank the anonymous reviewers for their critical comments, corrections, and thoughtful suggestions, which greatly improved the quality and comprehensiveness of this paper.

#### **Author Contributions**

Kapil, Gyanendra, and Dilendra contributed to the conceptualization and methodology of the study. Kapil, Gyanendra, and Rishi were responsible for data collection and site investigation. Kapil and Gyanendra contributed to data processing, interpretation, and prepared the original draft of the manuscript. Dilendra contributed to data curation and validation of result. Kapil, Dilendra, Gyanendra, Rishi, Praveen, Fahim, and Faraz were involved in review and editing. All authors reviewed and approved the final version of the article before submission.

# **Data Availability**

The data generated and analyzed during the current study are available from the corresponding author upon reasonable request. Additional data will be made available as part of ongoing collaborative research efforts.

#### **Declarations**

The authors declare no competing interests. The authors declare that they have no known competing financial interests or personal relationships that could have appeared to influence the work reported in this article.

### References

Acworth, R. I. (1987). The development of crystalline basement aquifers in a tropical environment.

Quarterly Journal of Engineering Geology, 20, 265–272.

https://doi.org/10.1144/GSL.QJEG.1987.020.04.02

Acharya, M., Shrestha, K. K., Bhandari, K., and Timilsina, A. (2023). Comparative study of two geophysical methods to investigate the depth of weak zone: A case study of Kulekhani-I Hydroelectric Project Dam, Makwanpur, Nepal. Journal of Earth Science and Climatic Change, 14(737), 2.

Adhikari, B., Acharya, U., Acharya, K., and Ghimire, S. (2019). Engineering geological investigation of dam site of proposed Sunkoshi-2 Hydropower Project, Khurkot area, eastern Nepal. Journal of Nepal Geological Society, 58, 181–188.

https://doi.org/10.3126/jngs.v58i0.24603

Aizebeokhai, A. P., Olayinka, A. I., and Singh, V. S. (2010). Application of 2D and 3D geoelectrical resistivity imaging for engineering site investigation in a crystalline basement terrain, southwestern Nigeria. Environmental Earth Sciences, 61(7), 1481–1492. https://doi.org/10.1007/s12665-010-0464-z

Alam, F., Alam, Q., Reza, S., Khurshid-ul-Alam, S. M., Saleque, K., and Chowdhury, H. (2017). A review of hydropower projects in Nepal. Energy Procedia, 110, 581–585.

https://doi.org/10.1016/j.egypro.2017.03.188

Al-Fares, W. (2011). Contribution of the geophysical methods in characterizing the water leakage in Afamia B Dam, Syria. Journal of Applied Geophysics, 75(3), 464–471.

https://doi.org/10.1016/j.jappgeo.2011.07.014

Argand, E. (1924). La tectonique de l'Asie. In Congrès Géologique International, Belgique, Comptes Rendus de la 13ème Session, en Belgique 1922 (pp. 171–372). Liège: H. Vaillant-Carmanne.

Binley, A., Hubbard, S. S., Huisman, J. A., Revil, A., Robinson, D. A., Singha, K., and Slater, L. D. (2015). The emergence of hydrogeophysics for improved understanding of subsurface processes over multiple scales. Water Resources Research, 51(6), 3837–3866. https://doi.org/10.1002/2015WR017016

- Burger, H. R., and Burger, D. C. (1992). Exploration geophysics of the shallow subsurface. New Jersey: Prentice-Hall.
- Cardarelli, E., Cercato, M., and Di Filippo, G. (2007). Assessing foundation stability and soil–structure interaction through integrated geophysical techniques: A case history in Rome (Italy). Near Surface Geophysics, 59(3), 244–259. https://doi:10.3997/1873-0604.2006026
- Cardarelli, E., Cercato, M., Cerreto, A., and Di Filippo, G. (2010). Electrical resistivity and seismic refraction tomography to detect buried cavities. Geophysical Prospecting, 58, 685–695.

https://doi.org/10.1111/j.1365-2478.2009.00854.x

- Central Water Commission (CWC). (2017). Bhakra Beas Management Board Report. Government of India.
- Chambers, J. C., Kuras, O., Meldrum, P. I., Ogilvy, R. D., and Hollands, J. (2006). Electrical resistivity tomography applied to geologic, hydrologic, and engineering investigations at a former waste disposal site. Geophysics, 71(6), B231–B239. https://doi.org/10.1190/1.2360184
- Colangelo, G., Lapenna, V., Loperte, A., Perrone, A., and Telesca, L. (2008). 2D electrical resistivity tomographies for investigating recent activation landslides in Basilicata region (southern Italy). Annals of Geophysics, 51(1), 12. https://doi.org/10.4401/ag-3048
- Colchen, M., and Le Fort, A. (1986). Annapurna– Manaslu–Ganesh Himal: Notice de la carte géologique au 1/200,000e (Bilingual ed.). Paris: Centre National de la Recherche Scientifique.
- Cubbage, B., Noonan, G. E., and Rucker, D. F. (2017). A modified Wenner array for efficient use of eight-channel resistivity meters. Pure and Applied Geophysics, 174(7), 2705–2718. https://doi.org/10.1007/s00024-017-1535-9
- De Groot-Hedlin, C., and Constable, S. (1990). Occam's inversion to generate smooth, twodimensional models from magnetotelluric data. Geophysics, 55, 1613–1624. https://doi.org/10.1190/1.1442813
- Demanet, D., Renardy, F., Vanneste, K., Jongmans, D., Camelbeeck, T. and Meghraoui, M. (2001). The use of geophysical prospecting for imaging active faults in the Roer Graben, Belgium. Geophysics, 66, 78–89. https://doi.org/10.1190/1.1444925
- Dewey, J. F., and Bird, J. M. (1970). Mountain belts and new global tectonics. Journal of Geophysical Research, 75, 2625–2685.

https://doi.org/10.1029/jb075i014p02625

Dobrin, M. B. (1982). Introduction to geophysical prospecting (3rd ed.). New Delhi: McGraw–Hill.

- Epting, J., Huggenberger, P., and Glur, L. (2009). A concept for integrated investigations of karst phenomena in urban environments. Engineering Geology, 109(3–4), 273–285. https://doi.org/10.1016/j.enggeo.2009.08.013
- Falae, P. O., Kanungo, D. P., Chauhan, P. K. S., et al. (2019). Electrical resistivity tomography (ERT) based subsurface characterisation of Pakhi landslide, Garhwal Himalayas, India. Environmental Earth Sciences, 78, 430. https://doi.org/10.1007/s12665-019-8430-x
- Fuchs, G. (1974). On the geology of the Karnali and Dolpo regions, west Nepal. Mitteilungen der Geologischen Gesellschaft in Wien, 66–67, 21–35.
- Fuchs, G. (1977). The geology of the Karnali and Dolpo regions, western Nepal. Jahrbuch der Geologischen Bundesanstalt, Wien, 120(2), 1–103.
- Ghimire, H., Bhusal, U. C., Khatiwada, B., and Pandey, D. (2017). Geophysical investigation using two-dimensional electrical resistivity tomography method to delineate subsurface geological structures at Dudhkoshi-II (230 MW) Hydroelectric Project, Solukhumbu District, Eastern Nepal. Journal of Nepal Geological Society, 55, 45–56.
- Griffiths, D. H., and Barker, R. D. (1993). Two-dimensional resistivity imaging and modeling in areas of complex geology. Journal of Applied Geophysics, 29, 21–26. https://doi.org/10.1016/0926-9851(93)90005-J
- Ha, H. S., Kim, D. S., and Park, I. J. (2010). Application of electrical resistivity techniques to detect weak and fracture zones during underground construction. Environmental Earth Sciences, 60, 723–731. https://doi.org/10.1007/s12665-009-0210-6
- Hagen, T. (1969). Report on the Geological Survey of Nepal. Vol. 1: Preliminary Reconnaissance. Mémoires de la Société Helvétique des Sciences Naturelles, 86(1), 185 pp.
- Hasan, M., Shang, Y., and Jin, W. J. (2018). Delineation of weathered/fracture zones for aquifer potential using an integrated geophysical approach: A case study from South China. Journal of Applied Geophysics, 157, 47–60.
  - https://doi.org/10.1016/j.jappgeo.2018.06.017
- Hasan, M., Shang, Y., Jin, W. J., and Akhter, G. (2020). An engineering site investigation using a non-invasive geophysical approach. Environmental Earth Sciences, 79, 265. https://doi.org/10.1007/S12665-020-09013-3
- Hassan Imam, M. D., Hossain, D., and Woobaid Ullah. (2013). Geoelectrical resistivity survey for the evaluation of hydrogeological condition of Bagerhat Sadar and the adjacent areas, Bangladesh. Journal of the Geological Society of India, 82, 290–294. https://doi.org/10.1007/s12594-013-0152-1

- Huayllazo, Y., Infa, R., Soto, J., Lazarte, K., Huanca, J., Alvarez, Y., and Teixidó, T. (2023). Using electrical resistivity tomography method to determine the inner 3D geometry and the main runoff directions of the large active landslide of Pie de Cuesta in the Vítor Valley (Peru). Geosciences, 13, 342. https://doi.org/10.3390/geosciences13110342
- Hubbard, S. S., and Rubin, Y. (2000). Hydrogeological parameter estimation using geophysical data: A review of selected techniques. Journal of Contaminant Hydrology, 45(1–2), 3–34. https://doi.org/10.1016/S0169-7722(00)00117-0
- Hung, Y.-C., Chou, H.-S., and Lin, C.-P. (2020).
  Appraisal of the spatial resolution of 2D electrical resistivity tomography for geotechnical investigation.
  Applied Sciences, 10, 4394.
  https://doi.org/10.3390/app10124394
- Jhinkwan, V. S., Chore, H. S., and Agnihotri, A. K. (2025, October). Application of electrical resistivity tomography (ERT) for the evaluation of slope susceptibility: A review. In International Conference on Environmental Geotechnology, Recycled Waste Materials and Sustainable Engineering (pp. 215–224). Singapore: Springer Nature Singapore. https://doi.org/10.1007/978-981-97-8393-9\_20
- Khalil, M. H. (2006). Geoelectric resistivity sounding for delineating saltwater intrusion in the Abu Zanima area, West Sinai, Egypt. Journal of Geophysics and Engineering, 3, 243–251.

https://doi.org/10.1088/1742-2132/3/3/006

- Kim, J. H., Yi, M. J., Song, Y., Seol, S. J., and Kim, K. S. (2007). Application of geophysical methods to the safety analysis of an earth dam. Journal of Environmental and Engineering Geophysics, 12, 221–235. https://doi.org/10.2113/JEEG12.2.221
- Kneisel, C. (2006). Assessment of subsurface lithology in mountain environments using 2D resistivity imaging. Geomorphology, 80(1–2), 32–44. https://doi.org/10.1016/j.geomorph.2005.09.012
- Kohn, M. J. (2014). Himalayan metamorphism and its tectonic implications. Annual Review of Earth and Planetary Sciences, 42, 381–419. https://doi.org/10.1146/annurev-earth-060313-055005
- Kumar, R. (2022). Case 16: Three Gorges Dam—The world's largest hydroelectric plant. In Sustainable Hydropower in Developing Countries (pp. 423–439). Springer. https://doi.org/10.1007/978-3-030-96725-3\_20
- Law, R. D., Searle, M. P., and Simpson, R. L. (2004). Strain, deformation temperatures, and vorticity of flow at the top of the Greater Himalayan slab, Everest Massif, Tibet. Journal of the Geological Society, 161, 305–320. https://doi.org/10.1144/0016-764903-047

- Lapenna, V., Lorenzo, P., Perrone, A., Piscitelli, S., Rizzo, E., and Sdao, F. (2005). 2D electrical resistivity imaging of some complex landslides in the Lucania Apennine chain, southern Italy. Geophysics, 70(3), G27–G36. https://doi.org/10.1190/1.1926571
- Lamsal, I., Ghimire, S., and Acharya, K. (2020).
  Geological and geophysical study in Udheri Khola area, Nalgad Hydroelectric Project, Jajarkot District, Lesser Himalaya, Western Nepal. Bulletin of the Department of Geology, 22, 11–16.
  <a href="https://doi.org/10.3126/bdg.v22i0.33409">https://doi.org/10.3126/bdg.v22i0.33409</a>
- Lech, M., Skutnik, Z., Bajda, M., and Markowska-Lech, K. (2020). Applications of electrical resistivity surveys in solving selected geotechnical and environmental problems. Applied Sciences, 10(17), 2263. https://doi.org/10.3390/app10072263
- Le Fort, P. (1975a). Himalaya: The collided range.
  Present knowledge of the continental arc. American
  Journal of Science, 275A, 1–44.
- Le Fort, P. (1996). Evolution of the Himalaya. In A. Yin and T. M. Harrison (Eds.), The tectonics of Asia (pp. 95–106). Cambridge University Press.
- Lin, C.-H., Lin, C.-P., Hung, Y.-C., Chung, C.-C., Wu, P.-L., and Liu, H.-C. (2018). Application of geophysical methods in a dam project: Life cycle perspective and Taiwan experience. Journal of Applied Geophysics, 158, 1–12.

https://doi.org/10.1016/j.jappgeo.2018.07.012

- Loke, M. H., Chambers, J. E., Rucker, D. F., Kuras, O., and Wilkinson, P. B. (2013). Recent developments in the direct-current geoelectrical imaging method. Journal of Applied Geophysics, 95, 135–156. https://doi.org/10.1016/j.jappgeo.2013.02.017
- Loke, M. H., and Barker, R. D. (1996). Rapid least-squares inversion of apparent resistivity pseudosections by a quasi-Newton method. Geophysical Prospecting, 44(1), 131–152. https://doi.org/10.1111/j.1365-2478.1996.tb00142.x
- Loke, M. H., Acworth, I., and Dahlin, T. (2003). A comparison of smooth and blocky inversion methods in 2-D electrical imaging surveys. Exploration Geophysics, 34(3), 182–187. https://doi.org/10.1071/EG03182
- Loperte, A., Soldovieri, F., Palombo, A., Santini, F., and Lapenna, V. (2016). An integrated geophysical approach for water infiltration detection and characterization at Monte Cotugno rock-fall dam (southern Italy). Engineering Geology, 211, 162–170. https://doi.org/10.1016/j.enggeo.2016.07.018
- Magnekou Takamte, C. R., Ntomba, S. M., Okomo Atouba, L. C., et al. (2022). Geophysical and geological considerations for characterizing the dam foundation during the Memve'ele dam construction (southern Cameroon): Influence on the dam type

- retained. Environmental Earth Sciences, 81, 343. https://doi.org/10.1007/s12665-022-10463-0
- Marescot, L., Monnet, R., and Chapellier, D. (2008). Resistivity and induced polarization surveys for slope instability studies in the Swiss Alps. Engineering Geology, 98(1–2), 18–28.

https://doi.org/10.1016/j.enggeo.2008.01.010

McGrath, R. J., Styles, P., Thomas, E., and Neale, S. (2002). Integrated high-resolution geophysical investigations as potential tools for water resource investigations in karst terrain. Environmental Geology, 42, 552–557.

https://doi.org/10.1007/s00254-001-0519-2

- Miller, C. R., Routh, P. S., Brosten, T. R., and McNamara, J. P. (2008). Application of time-lapse ERT imaging to watershed characterization. Geophysics, 73(3), G7–G17. https://doi.org/10.1190/1.2907156
- Montomoli, C., Carosi, R., and Iaccarino, S. (2015). Tectonometamorphic discontinuities in the Greater Himalayan Sequence: A local or a regional feature? Geological Society, London, Special Publications, 412, 25–41. https://doi.org/10.1144/SP412.3
- Mukhopadhyay, S., Tyagi, C., and Rai, S. S. (2006). The attenuation mechanism of seismic waves in Northwestern Himalayas. International Geophysical Journal, 167, 354–360.

https://doi.org/10.1111/j.1365-246X.2006.03117.x

- Nassim, H., Atmane, L., Lamine, H., Mouloud, H., and Anes, M. (2024). Integrated geotechnical and electrical resistivity tomography to map the lithological variability involved and breaking surface evolution in landslide context: A case study of the Targa Ouzemour (Béjaia). Water, 16(4), 682. https://doi.org/10.3390/w16050682
- Nepal Electricity Authority (NEA). (2020). Annual report 2019/20.
- NS Energy. (2025). Three Gorges Dam Hydropower Station. Retrieved June 19, 2025, from https://www.nsenergybusiness.com/projects/threegorges-dam-hydropower-station
- Pant, R. S. (2005). Application of 2D-ERT in feasibility study of hydropower projects in Nepal. In Symposium on the Application of Geophysics to Engineering and Environmental Problems 2005 (pp. 344–357). https://doi.org/10.4133/1.2923480
- Powell, C. M., and Conaghan, P. J. (1973). Plate tectonics and the Himalayas. Earth and Planetary Science Letters, 20(1), 1–12. https://doi.org/10.1016/0012-821X(73)90134-9
- Rehfeldt, K. R., Boggs, J. M., and Gelhar, L. W. (1992). Field study of dispersion in a heterogeneous aquifer: 3. Geostatistical analysis of hydraulic conductivity. Water Resources Research, 28(12), 3309–3324. https://doi.org/10.1029/92WR01758

- Rubin, Y., Mavko, G., and Harris, J. (1992). Mapping permeability in heterogeneous aquifers using hydrologic and seismic data. Water Resources Research, 28(7), 1809–1816. https://doi.org/10.1029/92WR00154
- Rucker, D. F., Noonan, G. E., and Greenwood, W. J. (2011). Electrical resistivity in support of geological mapping along the Panama Canal. Engineering Geology, 117(1–2), 121–133. https://doi.org/10.1016/j.enggeo.2010.10.012
- Samouëlian, I., Cousin, A., Tabbagh, A., Bruand, G., and Richard, G. (2005). Electrical resistivity survey in soil science: A review. Soil and Tillage Research, 83(2), 173–193.

https://doi.org/10.1016/j.still.2004.10.004

Satyabala, S. P., and Bilham, R. (2006). Surface deformation and subsurface slip of the 28 March 1999 Mw = 6.4 West Himalaya Chamoli earthquake, from InSAR analysis. Geophysical Research Letters, 33(23), L23305.

https://doi.org/10.1029/2006gl027422

- Sharma, R. H., and Awal, R. (2013). Hydropower development in Nepal. Renewable and Sustainable Energy Reviews, 21, 684–693.
  - https://doi.org/10.1016/j.rser.2013.01.013
- Singha, K., Day-Lewis, F. D., Johnson, T., and Slater, L. D. (2015). Advances in interpretation of subsurface processes with time-lapse electrical imaging. Hydrological Processes, 29(6), 1549–1576. https://doi.org/10.1002/hyp.10280
- Sigdel, A., Dhakal, P., Silwal, C. B., and Acharya, S. (2025). Slope stability assessment of Ramche and Dhaibung landslides in Central Nepal using geological, geophysical, and geotechnical approaches. Contributions to Geophysics and Geodesy, 55(3), 265–296.

https://doi.org/10.31577/congeo.2025.55.3.1

- Srivastava, H., Tiwari, R., Vijay, and Singh, D. (2022). A review on various geotechnical and geophysical investigations for a dam rehabilitation project. In Dam Engineering for the Future (pp. xxx–xxx). Springer. https://doi.org/10.1007/978-981-19-4739-1\_8
- Suzuki, K., Toda, S., Kusunoki, K., Fujimitsu, Y., Mogi, T., and Jomori, A. (2000). Case studies of electrical and electromagnetic methods applied to mapping active faults beneath thick Quaternary sediments. Engineering Geology, 56(1–2), 29–45. https://doi.org/10.1016/S0013-7952(99)00132-5
- Soupois, P. M., Georgakopoulos, P., Papadopoulos, N., Saltos, V., Andreadakis, A., Vallianatos, F., Sanis, A., and Makris, J. P. (2007). Use of engineering geophysics to investigate a site for a building foundation. Journal of Geophysics and Engineering, 4(2), 94–103. https://doi.org/10.1088/1742-2132/4/1/011

- SSE (Scottish and Southern Energy). (2009). Glendoe Hydro Scheme Overview.
- Telford, W. M., Geldart, L. P., and Sheriff, R. E. (1990). Applied geophysics (2nd ed.). Cambridge University Press.
- Tejero, A., Chávez, R. E., Urbieta, J., and Flores-Márquez, E. L. (2002). Cavity detection in the southwestern hilly portion of Mexico City by resistivity imaging. Journal of Environmental and Engineering Geophysics, 7(3), 130–139. https://doi.org/10.4133/jeeg7.3.130
- Thompson, S., Kulessa, B., Benn, D., et al. (2017). Anatomy of terminal moraine segments and implied lake stability on Ngozumpa Glacier, Nepal, from electrical resistivity tomography (ERT). Scientific Reports, 7, 46766.

https://doi.org/10.1038/srep46766

- U.S. Geological Survey (USGS). (2018). Three Gorges Dam: The world's largest hydroelectric plant. Retrieved June 19, 2025, from https://www.usgs.gov/special-topics/water-science-school/science/three-gorges-dam-worlds-largest-hydroelectric-plant
- Viviroli, D., Dürr, H. H., Messerli, B., Meybeck, M., and Weingartner, R. (2007). Mountains of the world, water towers for humanity: Typology, mapping, and global significance. Water Resources Research, 43, W07447. https://doi.org/10.1029/2006WR005653
- Viviroli, D., and Weingartner, R. (2008). "Water towers"—A global view of the hydrological importance of mountains. In E. Wiegandt (Ed.), Mountains: Sources of water, sources of knowledge (pp. 15–30). Springer. https://doi.org/10.1007/978-1-4020-6748-8 2
- Water and Energy Commission Secretariat (WECS). (2019). Assessment of hydropower potential of Nepal.
- Wise'n, R., Bjelm, L., and Dahlin, T. (2000). Resistivity imaging as a pre-investigation method in urban environments. In Proceedings EEGS-ES 6th Meeting (CH05). https://doi.org/10.3997/2214-4609.201406221
- Wu, J., Dai, F., Liu, P., et al. (2023). Application of electrical resistivity tomography in groundwater detection on the Loess Plateau. Scientific Reports, 13, 4821. https://doi.org/10.1038/s41598-023-31952-7